DOI: 10.1002/ejic.200600297

(Cyclen– and cyclam–pyridine)copper Complexes: The Role of the Pyridine Moiety in Cu^{II} and Cu^{I} Stabilisation

Sanae El Ghachtouli,[a] Cyril Cadiou,[a] Isabelle Déchamps-Olivier,[a] Françoise Chuburu,*[a] Michel Aplincourt,[a] and Thierry Roisnel[b]

Keywords: Copper / Cyclen and cyclam ligands / X-ray diffraction / UV/Vis and EPR spectroscopy / Electrochemistry / Configurational isomerisation

The protonation constants of cyclen– and cyclam–pyridine [1-(pyridin-2-ylmethyl)-1,4,7,10-tetraazacyclododecane ($\mathbf{L^1}$) and 1-(pyridin-2-ylmethyl)-1,4,8,11-tetraazacyclotetradecane ($\mathbf{L^2}$), respectively] and the stability constants ($\log\beta_{110}$) of the corresponding copper complexes ($[Cu\mathbf{L^1}]^{2+}$ and $[Cu\mathbf{L^2}]^{2+}$) were determined by potentiometric titrations. The complexes were subsequently isolated and characterised by X-ray diffraction, UV/Vis spectroscopy and electrochemical studies. The $[Cu\mathbf{L^2}]^{2+}$ complex adopts two distinct and stable geometries (*trans* I and III), which mainly differ by the macrocycle configuration. The *trans* III configurational isomer can be converted into the *trans* I one by electron transfer.

Introduction

The coordination chemistry of tetraazamacrocyclic receptors like cyclen and cyclam is always of interest, as new fields like diagnostic imaging or therapeutic agent development have recourse to such ligands. Gadolinium complexes of polyamino carboxylate ligands are frequently used as contrast agents for magnetic resonance imaging (MRI) to improve the images.[1] Therapeutic metalloradiopharmaceuticals designed to localise tumour sites and deliver a cytotoxic radiation dose have become widespread.[2] These molecules are made up of a bifunctional chelator, which coordinates the metal ion and is covalently attached to a targeting molecule. The design of the chelator depends on the metal ion and, for instance, the complexation of copper radionucleides is provided by *N*-functionalised cyclams.[3] High thermodynamic and kinetic complex stabilities constitute crucial parameters for their in vivo applications. For this purpose, tetraazamacrocyclic receptors are very well suited, as the donor atoms, the ligand denticity and, above all, the ligand preorganisation ensure such stabilities. Finally, stereochemistry is often important when targeting complexes to specific receptors and, as far as tetraazamacrocyclic ligands are concerned, the orientation of the N–H bonds is important for receptor recognition.[4] It was recently shown that modifications of the macrocyclic substitution pattern can act directly on the stereochemistry and the properties of the metal complexes.[5–7] In particular, in metal complexes of *N*,*N*′,*N*′′,*N*′′′-tetrasubstituted tetraazamacrocycles, topological reorganisations can be induced by electron transfer. For these reasons, the preparation and characterisation of coordination compounds with tetraazamacrocyclic ligands bearing pendant substituents are still of interest. *N*-functionalisation may enhance the metal complexation and the coordination ability of the pendant arms may affect the stereochemistry of the metal complexes.

In this study, we focused on the copper coordination of cyclen– and cyclam–pyridine ($\mathbf{L^1}$ and $\mathbf{L^2}$, respectively; Scheme 1) in aqueous solution. The stability constants of the 1:1 copper complexes were determined. The complexes' stereochemistry was studied in solution (UV/Vis and EPR measurements) and supported by X-ray data. Finally, electrochemical experiments were carried out to give an insight into the behaviour of the copper complexes in solution.

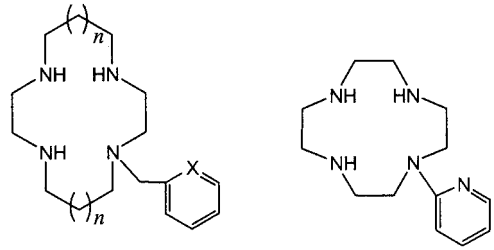

X = N: $n = 0$ $\mathbf{L^1}$; $n = 1$ $\mathbf{L^2}$

X = C: $n = 0$ $\mathbf{L^4}$; $n = 1$ $\mathbf{L^5}$

$\mathbf{L^3}$

Scheme 1.

[a] GRECI, Université de Reims Champagne-Ardenne, B. P. 1039, 51687 Reims Cedex 2, France
[b] UMR CNRS 6511, Institut de Chimie de Rennes, CS 74205, 35042 Rennes Cedex, France
E-mail: francoise.chuburu@univ-reims.fr
Supporting information for this article is available on the WWW under http://www.eurjic.org or from the author.

Results and Discussion

The ligands **L¹** and **L²** were prepared according to the bis(aminal) methodology.[8] The protonation constants of the ligands and the overall formation constants of the copper complexes (see Experimental Section) were determined by means of potentiometric titrations at 20 °C in a 1 mol·L^{-1} KNO_3 medium.

Acid/Base Behaviour of L¹ and L²

The titration of the **L¹** and **L²** solutions gave rise to neutralisation curves with a single inflexion point at pH ≈ 7 for both ligands. A nonlinear least-squares refinement of six independent data sets with PROTAF software[9] allowed the determination of the $\log K_{01h}$ values, which are summarised in Table 1 with those of cyclen, cyclam and a monopyridyl relevant derivative, **L³** (Scheme 1), for comparison. For both ligands, one should expect five protonation constants, four for the nitrogen atoms of the macrocycle and one for the pyridinic nitrogen atom (N_{pyr}).

For **L¹**, the first two constants, $\log K_{011}$ (10.6) and $\log K_{012}$ (9.77), are close to those determined for the parent cyclen.[10] It means that the beginning of the protonation pattern of **L¹** is similar to the cyclen one and that the first two added protons are bound inside the macrocyclic cavity. The same proposal can be formulated for the cyclam analogue **L²**, as the first two protonation constants ($\log K_{011}$ = 11.31 and $\log K_{012}$ = 10.47) are similar to the ones determined for the parent cyclam.[11]

For **L¹**, only the third protonation constant ($\log K_{013}$ = 3.42) can be reached, while the last two are too weak to be determined with sufficient accuracy, unlike **L²**, for which three additional protonation constants ($\log K_{013}$ = 2.88, $\log K_{014}$ = 2.32 and $\log K_{015}$ = 1.73) are calculated. For each ligand, the purpose is to identify as much as possible when the N_{pyr}-protonation occurs. In fact, for the ligands incorporating a pyridine moiety, the N_{pyr}-protonation occurs in a wide pH range: for example the N_{pyr} protonation constant is $\log K_{012}$ = 2.46[12a] for the 2-pyridinylmethanamine, and $\log K_{013}$ = 3.91 for the relevant ligand cyclen–pyridine **L³** (Table 1[12b]). Consequently, for the studied ligands, the identification of the third (**L¹**) or third and fourth (**L²**) protonation sites remains ambiguous, as these protonation steps occur at pH < 3.5, and in this pH range at least two sites are in competition, the first one being the N_{pyr} atom, the second one being a nitrogen atom from the macrocyclic cavity. This is particularly true for the cyclam ligand **L²**. In order to gain an insight into the protonation pattern of **L¹** and **L²**, UV absorption and ^{1}H NMR evolutions taking place upon protonation were investigated. For **L¹** and **L²**, the acidification of the medium induces in the UV absorption spectra (Figure 1) the characteristic hyperchromic shift of the pyridine chromophore,[13] which begins to appear at pH = 3.7 for **L¹**, at pH = 2.9 for **L²** and increases with decreasing pH to a maximum for **L¹** at pH = 1.5 and for **L²** at pH = 1.6. The protonation patterns of **L¹** and **L²** ligands were then examined by recording ^{1}H NMR spectra at different pH values. The proton assignment was firstly elucidated with the help of two-dimensional ^{1}H-^{1}H COSY, ^{1}H-^{13}C HMQC and ^{1}H-^{13}C HMBC correlation charts. For **L¹** (Figure 2, see also SI-1 in the Supporting Information), the chemical shifts of the aromatic protons (H_{ar}) are sensitive reporters of the protonation state of the ligand amino

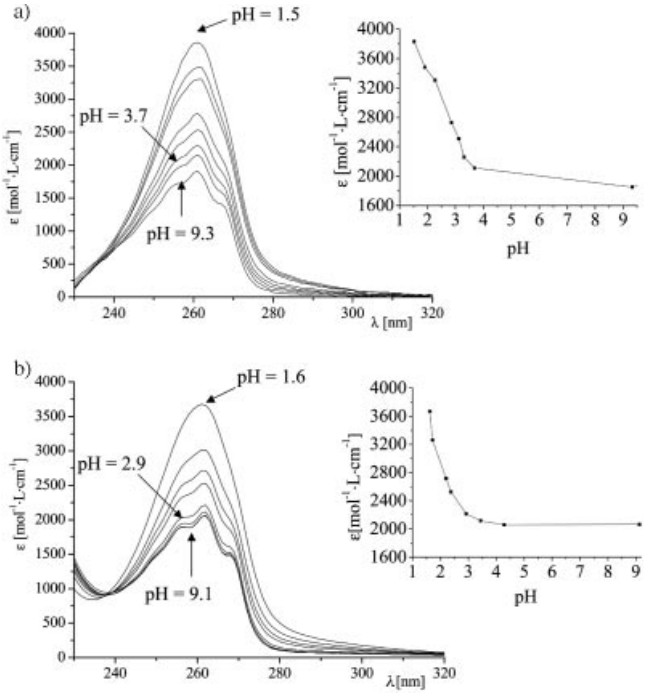

Figure 1. Spectrophotometric titrations of **L¹** and **L²** by KOH (0.1 mol·L^{-1}): (a) [**L¹**] = 3.9 × 10^{-4} mol·L^{-1} in HCl (1 mol·L^{-1}), pH ∈ [1.5; 9.3]. (b) [**L²**] = 2.34 × 10^{-4} mol·L^{-1} in HCl (1 mol·L^{-1}), pH ∈ [1.6; 9.1]. T = 20 °C; l = 1 cm [inset: ε (mol^{-1}·L·cm^{-1}) = f(pH)].

Table 1. Ligand protonation constants $\log K_{01h}$ and overall formation constants β_{110} of the 1:1 copper complexes. Values in parentheses represent 2σ standard deviation.

	L¹[a]	L²[a]	L³[b]	L⁴[a]	L⁵[a]	Cyclen[c]	Cyclam[c,d]
$L + H^+ \rightleftharpoons LH^+$	10.6(1)	11.31(1)	10.99(5)	10.80(6)	11.5(1)	10.97	11.58
$LH^+ + H^+ \rightleftharpoons LH_2^{2+}$	9.77(8)	10.47(6)	7.16(5)	9.23(3)	9.31(3)	9.87	10.62
$LH_2^{2+} + H^+ \rightleftharpoons LH_3^{3+}$	3.42(5)	2.88(8)	3.91(5)	<2	2.46(4)	<2	1.61
$LH_3^{3+} + H^+ \rightleftharpoons LH_4^{4+}$	<2	2.32(1)	<3	<2	2.29(7)	<2	2.42
$LH_4^{4+} + H^+ \rightleftharpoons LH_5^{5+}$	<2	1.73(5)					
$Cu^{2+} + L \rightleftharpoons CuL^{2+}$	21.0(2)	23.0(2)		20.4(3)	22.0(2)	23.3	26.5

[a] Potentiometric titrations experimented at 20.0(1) °C, I = 1 mol·L^{-1} (KNO_3) (this work). [b] Ref.[12b] at 25 °C, I = 0.1 mol·L^{-1} ($NaClO_4$). [c] Ref.[10] at 25 °C, I = 1 mol·L^{-1} (KNO_3). [d] Ref.[11]

functions. In the pH range 4–12, no significant evolution of the $^1H_{ar}$ chemical shifts is observed (see also molecular modelling of **L¹**), which means that the first two protons bind the macrocycle (**L¹**H⁺ and **L¹**H_2^{2+} species). In the pH range 2–4, a marked downfield shift is observed for the signals of the aromatic protons. This observation, in agreement with the UV data, strongly suggests that the third protonation step in **L¹** occurs on the N_{pyr} atom.[14] For **L²** (Figure 3, see also SI-2,3 in the Supporting Information), the best reporters of the protonation steps are the H_{ar} and the protons in the β-position with respect to the macrocyclic nitrogen atoms. In the pH range 9–12, a downfield shift is observed for the signals of the aliphatic protons, confirming that the first two protons added (species **L²**H⁺ and **L²**H_2^{2+}) bind to the macrocyclic cavity. In the pH range 1.5–3, a concomitant downfield shift of the signals of H_{ar} and β-H is observed. In this region, the distribution diagram of the protonated **L²** species indicates that the existence domains of **L²**H_3^{3+}, **L²**H_4^{4+} and **L²**H_5^{5+}overlap. It is worth noting that the coexistence of these three species induces a deep modification of the β-H signals with the coalescence of the β-H signals at pH ≈ 2 (see SI-3 of the Supporting Information). All these arguments mean that, for **L²**, the third and fourth protonation steps cannot be unambiguously attributed to the N_{pyr} atom and to a macrocyclic nitrogen atom, respectively.

It is worth noting too that, for **L¹**, the difference between $\log K_{012}$ and $\log K_{013}$ is important. The third protonation constant attributed to the N_{pyr} atom in **L¹** ($\log K_{013}$ = 3.42) is about two orders of magnitude smaller than that for the N_{pyr}-protonation in pyridine (pK_a = 5.25[15]). This difference reflects the free-energy cost of protonating the third amino group in **L¹**, that is, the protonation of the N_{pyr} atom is more difficult when the pyridine group is appended in proximity to the macrocyclic ring. At least two reasons can be invoked to explain this behaviour.[16] The first one takes into account the stabilisation of the diprotonated structure by intramolecular hydrogen bonding with the pyridine nitrogen atom (the protonation of this atom then induces hydrogen bond break-up). The second one corresponds to a conformational reorganisation upon protonation. To check these assumptions, molecular modelling of **L¹** and its protonated forms was undertaken.

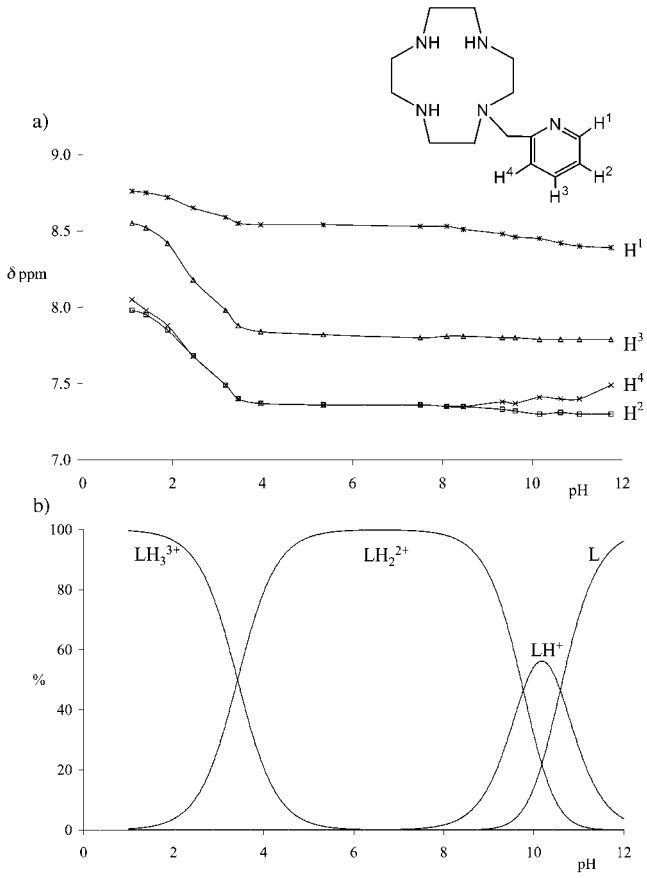

Figure 2. (a) pH dependence of the ^1H aromatic NMR signals of **L¹**. (b) Distribution diagram of the **L¹** protonated forms ([**L¹**] = 1.5×10^{-3} mol·L^{-1}, I = 1 mol·L^{-1}).

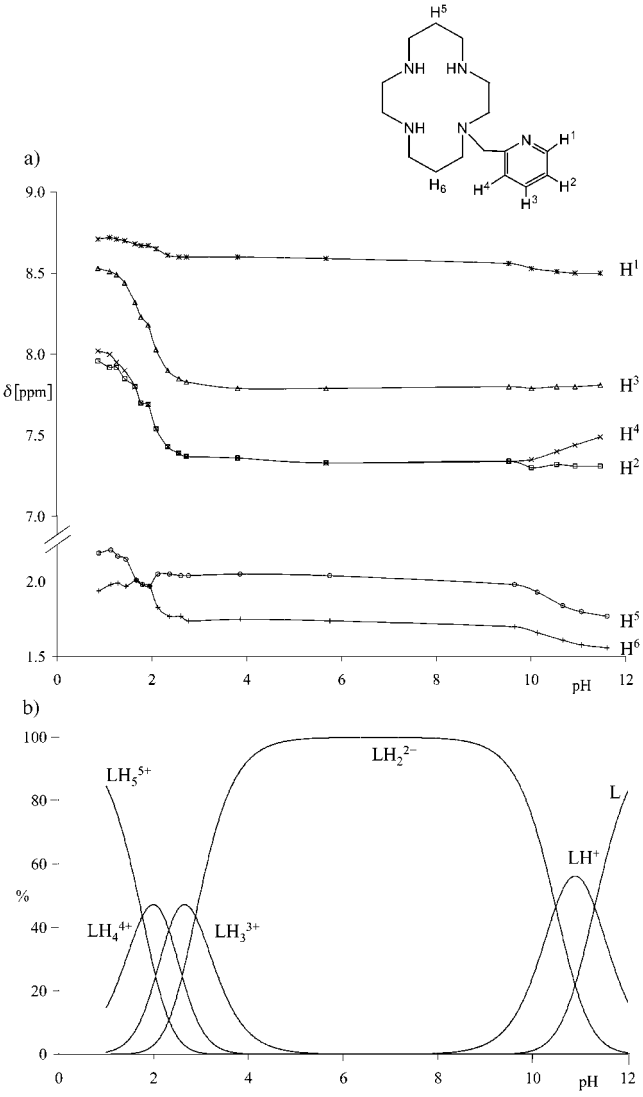

Figure 3. (a) pH dependence of the ^1H aromatic and β-H NMR signals of **L²**. (b) Distribution diagram of the **L²** protonated forms ([**L²**] = 1.5×10^{-3} mol·L^{-1}, I = 1 mol·L^{-1}).

Molecular Modelling of L^1 and Its Protonated Forms

Low-energy conformers generated by a conformational search performed at the semiempirical level (AM1 calculations) were optimised using the Gaussian package[17a] under DFT/B3LYP/6-31G* formalism. The results concerning the **L¹** ligand are gathered in Table 2.

Table 2. DFT-optimised molecular structures of **L¹**, $[\mathbf{L^1}H]^{1+}$, $[\mathbf{L^1}H_2]^{2+}$and $[\mathbf{L^1}H_3]^{3+}$. For the sake of clarity, only the pertinent hydrogen atoms are represented. The dashed lines correspond to hydrogen bonds.

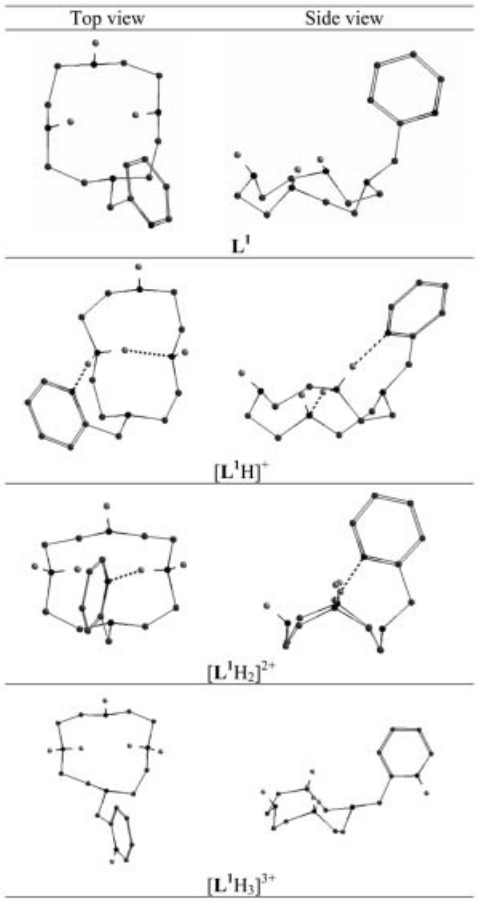

The lowest-energy structure computed for the neutral ligand **L¹** shows an outward orientation of the pyridine moiety relative to the macrocyclic cavity. The macrocycle has two of the three hydrogen atoms of the secondary amine functions directed towards the centre of the cavity. For the stepwise addition of protons, all the protonation sites were considered and the most stable situations are reported in Table 2. As the first proton is added, the pyridine moiety moves towards the inside of the macrocyclic cavity. The optimised geometry shows that the added proton is stabilised by a hydrogen bond with the N_{pyr} atom, the overall structure being stabilised by two intramolecular hydrogen bonds. These characteristics are reinforced when the addition of the second proton is considered. The diprotonated structure is symmetrical, the symmetry plane including the pyridine ring. The pyridine moiety is then in an apical position towards the macrocyclic cavity, the N_{pyr} atom stabilising the added proton by hydrogen bonds. Finally, the addition of the third proton occurs on the N_{pyr} atom and the pyridine moiety is moved outward the macrocyclic cavity. The N_{pyr} atom can no longer stabilise the first two added protons, as the hydrogen bonds are broken up. Moreover, the comparison of the calculated macrocyclic shapes for the **L¹** ligand and its protonated forms shows conformational modifications. The reorganisation of the macrocyclic cavity as a function of an increased number of protons is a way to accommodate positive charges in proximity. The modification is particularly important between $[\mathbf{L^1}H_2]^{2+}$ and $[\mathbf{L^1}H_3]^{3+}$ structures, as it corresponds to the shift of the pyridine ring away from the cyclen cavity. All these considerations indicate that the protonation of the $[\mathbf{L^1}H_2]^{2+}$ species is difficult, which is in good agreement with the small $\log K_{013}$ value determined for **L¹**.

Copper Complexation of L^1 and L^2

Thermodynamic Stability of the Complexes $[CuL^1]^{2+}$ and $[CuL^2]^{2+}$

The pH titration of the ligands **L¹** and **L²** in the presence of 1 equiv. of copper(II) showed the formation of $[Cu\mathbf{L^1}]^{2+}$ and $[Cu\mathbf{L^2}]^{2+}$ complexes. From the analysis of the titration data, the complexation constants $\log\beta_{110}$ of $[Cu\mathbf{L^1}]^{2+}$ (21.0 ± 0.2) and $[Cu\mathbf{L^2}]^{2+}$ (23.0 ± 0.2) were determined (Table 1). The comparison of these values with those determined for (cyclen)- and (cyclam)copper complexes shows that the *N*-functionalisation of the cavity provokes a decrease of the complexes' stability (Table 1). This decrease is, however, less pronounced than for the benzyl complexes $[Cu\mathbf{L^4}]^{2+}$ and $[Cu\mathbf{L^5}]^{2+}$ (Table 1). This suggests that in solution the pyridine moiety is weakly involved in copper coordination.

Molecular Structures of the Complexes

To provide a proof of the stoichiometry and the structure of the complexes, a crystallographic study of the copper(II) complexes of **L¹** and **L²** was carried out.

For the $[Cu\mathbf{L^1}]^{2+}$ complex, X-ray quality blue single crystals were grown from diffusion of diethyl ether into an acetonitrile solution of the complex. Selected geometrical parameters are given in Table 3. The X-ray structure of $[Cu\mathbf{L^1}]^{2+}$ showed that the metal ion is pentacoordinate (Figure 4), the coordination sphere of the copper centre consisting of the four macrocyclic nitrogen atoms and the pyridinic N_{pyr} atom. The Cu–N(secondary) bond lengths [2.013(4)–2.022(4) Å] are in the range expected for a copper ion coordinated in a cyclen cavity;[18] the Cu–N(tertiary) bond length of 2.058(3) Å, longer than the average of the Cu–N(secondary) ones (2.018 Å), is a consequence of the macrocyclic *N*-alkylation.[19] The N_{pyr} atom is coordinated to the copper ion and the Cu–N_{pyr} bond length is rather short [2.164(4) Å] by comparison with the same situation in the corresponding bis(macrocyclic) compound (2.266 Å).[18] This leads, in the solid state, to an efficient five-membered

chelate ring, as the N_{pyr}–Cu–N4 angle of 80.65(14)°, where the N4 atom bears the pyridine arm, is noticeably smaller than the other three N_{pyr}–Cu–N angles [99.00(17)–126.74(16)°].

Table 3. Selected bond lengths [Å] and angles [°] in $[CuL^1]^{2+}$.

Cu–N1	2.013(4)	N1–Cu–N2	86.31(16)
Cu–N2	2.020(4)	N1–Cu–N3	146.94(18)
Cu–N3	2.022(4)	N1–Cu–N4	85.44(14)
Cu–N4	2.058(3)	N1–Cu–N5	111.24(16)
Cu–N5	2.164(4)	N2–Cu–N3	86.10(16)
		N2–Cu–N4	152.46(17)
		N2–Cu–N5	126.74(16)
		N3–Cu–N4	86.62(15)
		N3–Cu–N5	99.00(17)
		N4–Cu–N5	80.65(14)

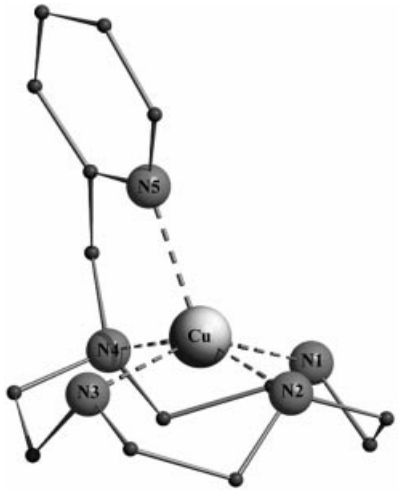

Figure 4. SCHAKAL diagram of $[CuL^1]^{2+}$.

For the $[CuL^2]^{2+}$ complex, as far as metal cation coordination by a cyclam derivative is concerned, one may expect the formation of stereoisomers for the complexes, according to the relative orientation of the NH group towards the macrocyclic cavity. The most frequently encountered configurational isomers are *trans* I (*R*,*S*,*R*,*S*) (++++) and *trans* III (*R*,*R*,*S*,*S*) (+–+–), where + indicates that the NH group is above the plane of the macrocycle and – indicates that it is below the plane.[20] Recently, it was demonstrated that, according to the redox state of the copper centre, different coordination modes around the metal ion are reached and can be responsible for the formation of the *trans* I and the *trans* III isomers.[6] Thus, depending on the experimental conditions, *trans* I and *trans* III isomers of $[CuL^2]^{2+}$ were isolated and characterised in the solid state. A $[CuL^2]^{2+}$ complex was easily obtained as a blue solid when the synthesis was performed with copper perchlorate in CH_3OH. The X-ray structure of the corresponding complex (Figure 5, Table 4a) showed that it adopts the *trans* I arrangement. The copper ion is pentacoordinate in a distorted square-pyramidal environment. The N_{pyr} atom is therefore coordinated to the metal centre [2.220(2) Å]. The bond angles around the copper ion are different from those expected in an ideal square-pyramidal structure [e.g. N1CuN2, N4CuN1, N2CuN4, N3CuN1 of 86.20(5), 95.83(5), 170.96(5), 164.19(5)°, respectively]. The four macrocyclic nitrogen atoms define a plane and the copper ion is out of this plane by 0.218 Å.

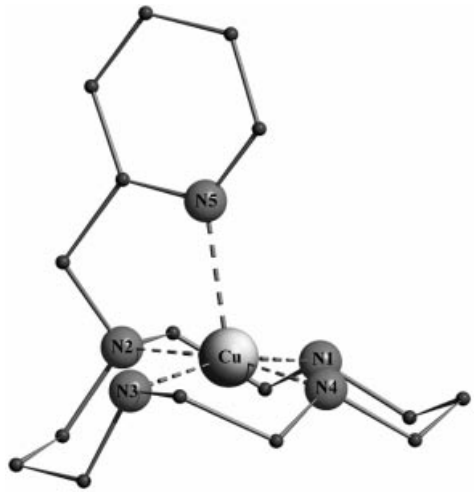

Figure 5. SCHAKAL diagram of $[CuL^2]^{2+}$ *trans* I.

Table 4. Selected bond lengths [Å] and angles [°] of $[CuL^2]^{2+}$ *trans* I (a) and $[CuL^2]^{2+}$ *trans* III (b).

a			
Cu–N1	2.010(2)	N1–Cu–N2	86.20(5)
Cu–N2	2.080(2)	N1–Cu–N3	164.19(5)
Cu–N3	2.024(2)	N1–Cu–N4	95.83(5)
Cu–N4	2.037(2)	N1–Cu–N5	95.39(5)
Cu–N5	2.220(2)	N2–Cu–N5	78.66(5)
		N3–Cu–N2	90.33(5)
		N3–Cu–N4	85.34(5)
		N3–Cu–N5	99.05(5)
		N4–Cu–N2	170.96(5)
		N4–Cu–N5	109.84(5)
b			
Cu–N1	2.038(2)	N1–Cu–N3	169.05(8)
Cu–N2	2.025(2)	N1–Cu–N5	109.70(8)
Cu–N3	2.092(2)	N2–Cu–N1	90.92(9)
Cu–N4	2.024(2)	N2–Cu–N3	85.64(9)
Cu–N5	2.250(2)	N2–Cu–N5	95.11(8)
		N3–Cu–N5	80.99(8)
		N4–Cu–N1	84.71(9)
		N4–Cu–N2	165.38(9)
		N4–Cu–N3	96.05(9)
		N4–Cu–N5	99.50(8)

When the complexation was performed with L^2 and $Cu(CH_3CN)_4PF_6$ as Cu^I salt in CH_3OH under aerobic conditions,[6] a violet solid resulting from the oxidation of Cu^I by dioxygen was formed. The X-ray structure of the complex (Figure 6, Table 4b) highlighted the fact that it adopts a *trans* III configuration. The copper environment is still pentacoordinate, the N_{pyr}–Cu bond being a little longer [2.250(2) Å] than the corresponding one in the *trans* I complex. The main geometrical parameters are more or less the same as those observed for the *trans* I isomer, the copper ion being out of the macrocyclic plane by 0.224 Å.

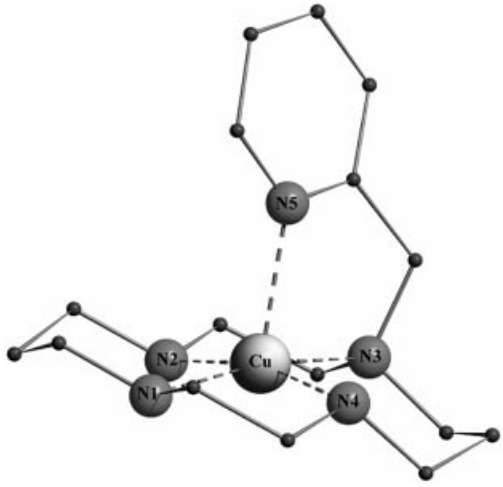

Figure 6. SCHAKAL diagram of $[CuL^2]^{2+}$ *trans* III.

UV/Vis Spectral Properties and EPR Studies of the $[CuL^{1,2}]^{2+}$ Complexes

The UV/Vis absorption maxima of the complexes $[CuL^{1,2}]^{2+}$ in water and in acetonitrile together with the corresponding solid-reflectance spectra are listed in Table 5.

Table 5. UV/Vis data $\{\lambda$ [nm] $(\varepsilon$ [mol^{-1}·L·cm^{-1}])$\}$ of $[CuL^{1,2}]^{2+}$ complexes in H_2O, CH_3CN solutions and in the solid state.

	H_2O	CH_3CN	Solid state
$[CuL^1]^{2+}$	595 (218)	601 (247)	600
$[CuL^2]^{2+}$ *trans* I	602 (129)	588 (144)	580
$[CuL^2]^{2+}$ *trans* III	541 (228)	550 (125)	551

In the $[CuL^2]^{2+}$ *trans* I/III complexes, with regard to the copper band, the spectrum of the *trans* I complex exhibits a λ_{max} = 602 nm in H_2O (588 nm in CH_3CN) and a λ_{max} = 580 nm in the solid state. The concordance of solid-state and solution UV/Vis spectra means that on going from the solid state to solution, the copper environment is maintained. The λ_{max} values are consistent with a pentacoordinate copper centre,[19b,21] where the pyridyl group coordination has to be considered, according to the X-ray data for the $[CuL^2]^{2+}$ *trans* I complex (CuN_5 chromophore). For the *trans* III complex, a λ_{max} = 541 nm in H_2O (550 nm in CH_3CN) and a λ_{max} = 551 nm in the solid state were determined. The λ_{max} values suggest then that the pyridyl group in the *trans* III complex is still coordinated to the metal centre (CuN_5 chromophore). When a 5 M perchloric acid solution was added to aqueous solutions of $[CuL^2]^{2+}$ *trans* I/III complexes, a blue shift was observed for the absorption maxima (from 602 to 531 nm for $[CuL^2]^{2+}$ *trans* I and from 541 to 511 nm for $[CuL^2]^{2+}$ *trans* III). The positions of the resulting bands (531 and 511 nm) are typical of a CuN_4 chromophore where the metal ion is held in an *N*-monofunctionalised cyclam cavity.[22] Then the acid addition triggered the pyridine decoordination.

In the $[CuL^1]^{2+}$ complex, the spectrum exhibits a broad band at λ_{max} = 595 nm in H_2O (601 nm in CH_3CN) and at λ_{max} = 600 nm in the solid state. The positions of these bands are typical of a square-pyramidal complex[18] where the copper centre is pentacoordinate. The concordance of solid-state and solution UV/Vis spectra seems to indicate that the copper coordination is again the same in the solid state and in solution. On the basis of the X-ray structure, it means that the pyridine moiety participates in the metal coordination (CuN_5 chromophore). To test this proposal, a 5 M perchloric acid solution was added to an aqueous solution of the $[CuL^1]^{2+}$ complex. Under these conditions, no blue shift of the absorption maximum was observed. In fact, this is not surprising if we consider that under acidic conditions the pyridine moiety can be decoordinated and replaced by a water molecule, as it is well known that in the cyclen cavity the copper ion is always pentacoordinate.[18] The acidification of the $[CuL^1]^{2+}$ solution can lead to chromophore modification from CuN_5 to CuN_4O.

Electron paramagnetic resonance corroborates the coordination geometry proposed for the copper ion in $CuL^1]^{2+}$ and $[CuL^2]^{2+}$ *trans* I/III complexes. The EPR spectra of the three complexes were recorded in a DMF solution at 150 K to ensure good glasses, and the corresponding simulated anisotropic parameters are listed in Table 6. The X-band EPR spectra of $[CuL^1]^{2+}$ and $[CuL^2]^{2+}$ *trans* I/III frozen solutions exhibit a strong absorption at about 3200 G, imputable to the allowed transitions $\Delta M_S = 1$. The shapes of the spectra consisted of four equidistant absorptions in the parallel region as expected for the coupling of the unpaired copper electron to the copper nucleus (I = 3/2) (SI-4 in the Supporting Information). These spectra with $g_\parallel > g_\perp$ and $G > 4$ are typical of axially symmetric d^9 copper(II) complexes in a ground-state doublet with the unpaired electron in the $d_{x^2-y^2}$ orbital.[21] Moreover, for $[CuL^2]^{2+}$ complexes, the $g_\parallel$ values are slightly larger than that for [Cu(cyclam)]$^{2+}$ (2.186),[23] which is again consistent with the *N*-alkylation of the macrocyclic cavity.[22] The hyperfine coupling constant $A_\parallel$ is also a good indicator of distortion from square-planar to square-pyramidal coordination in copper(II) complexes, with smaller values implying distortion.

Table 6. EPR parameters of $[CuL^{1,2}]^{2+}$ complexes in frozen solution (DMF) at 150 K.

	$g_\parallel$	$g_\perp$	[a]	$A_\parallel$ [10^{-4} cm^{-1}]	$A_\perp$ [10^{-4} cm^{-1}]
$[CuL^1]^{2+}$	2.192	2.045	4.26	175.0	15.6
$[CuL^2]^{2+}$ *trans* I	2.190	2.045	4.22	177.5	25.5
$[CuL^2]^{2+}$ *trans* III	2.197	2.045	4.37	188.7	22.5
[Cu(cyclen)]$^{2+}$[b]	2.198	2.057		184	
[Cu(cyclam)]$^{2+}$[b]	2.186	2.049		205	

[a] $G = (g_\parallel - 2)/(g_\perp - 2)$. [b] Ref.[23]

The $A_{\parallel}$ values for $[Cu\mathbf{L^1}]^{2+}$and $[Cu\mathbf{L^2}]^{2+}$ *trans* I/III are smaller than the corresponding $A_{\parallel}$ values for $[Cu(cyclen)]^{2+}$ and $[Cu(cyclam)]^{2+}$ (Table 6), which is consistent with $[Cu\mathbf{L^1}]^{2+}$and $[Cu\mathbf{L^2}]^{2+}$ *trans* I/III X-ray structures and pentacoordinate copper centres.

Redox Properties of the $[CuL^{1,2}]^{2+}$ Complex

The electrochemical behaviour of $[Cu\mathbf{L^1}]^{2+}$ in acetonitrile was determined. The reduction was quasireversible and occurred at $E_{1/2}^{red}$ = –0.89 V versus Fc^+/Fc (ΔE_p = 80 mV); the oxidation was irreversible with a peak potential at E_p^{ox} = 1.55 V versus Fc^+/Fc. No change in the CV waves was observed when full scans were performed except a drop in the current intensities when the system was investigated at high potentials, because of the irreversible oxidation.

Electrochemical studies of acetonitrile solutions of $[Cu\mathbf{L^2}]^{2+}$ *trans* I/III were only performed on the Cu^{II}/Cu^{I} reduction system as oxidation to Cu^{III} is irreversible and produces highly oxidative species giving very high anodic currents.[24] For the *trans* I complex, a single quasireversible reduction system was observed at $E_{1/2}^{red}$ = –1.145 V versus Fc^+/Fc (ΔE_p = 130 mV) and the voltammogram was fully reproducible from the first scan to several scans in reduction. This means that the electrogenerated $[Cu\mathbf{L^2}]^{+}$ *trans* I complex is stable, as it does not evolve within the voltammetry timescale.[7] For the *trans* III complex, the reduction yielded the short-lived $[Cu\mathbf{L^2}]^{+}$ *trans* III complex, for which an irreversible wave was located at E_p^{red} = –1.05 V versus Fc^+/Fc. The comparison of the reduction potential of $[Cu\mathbf{L^2}]^{2+}$ *trans* I and $[Cu\mathbf{L^2}]^{2+}$ *trans* III shows that the *trans* I complex is more difficult to reduce than the *trans* III one. This has to be correlated with the Cu–N_{pyr} distances obtained from crystallographic measurements. For the *trans* I complex, the Cu–N_{pyr} distance is 2.220 Å, while for the *trans* III one this distance is 2.250 Å; for the *trans* I isomer, the ligand field is therefore stronger. Consequently, the *trans* I isomer's antibonding e_g* orbitals are destabilised compared to the *trans* III ones, making, for the *trans* I isomer, the removal of an electron easier and its withdrawal more difficult.[22]

The electrogenerated $[Cu\mathbf{L^2}]^{+}$ *trans* III complex is a transient species. Effectively, it readily isomerises as the reversible *trans* I system at $E_{1/2}^{red}$ = –1.15 V versus Fc^+/Fc (ΔE_p = 140 mV) is immediately observed after the irreversible *trans* III one. On cycling, the consecutive voltammograms exhibit only the *trans* I system. This behaviour has been observed until now only on tetrasubstituted (cyclam)copper complexes,[6,7] and indicates that the topological rearrangement process of the electrogenerated $[Cu\mathbf{L^2}]^{+}$ *trans* III complex to a $[Cu\mathbf{L^2}]^{+}$ *trans* I complex is rapid. One can also conclude that the pyridine moiety greatly enhances the $[Cu\mathbf{L^2}]^{+}$ stabilities, particularly for the *trans* I complex, as it does not evolve towards other species within the voltammetry timescale.[7] Finally, as the *trans* III → *trans* I conversion has not been observed by other techniques, electrochemical experiments illustrate the relevance of electron transfer in mediating topological reorganisation of the functionalised cyclam cavity.

Conclusion

In cyclen– and cyclam–pyridine ligands and their copper complexes, the pyridine moiety behaves as a "non-innocent" fragment and its influence can be felt at several levels.

In the ligands, it participates through intramolecular hydrogen bonds in the stabilisation of two added protons in the macrocyclic cavity. In the copper complexes, the pyridine nitrogen atom participates as a fifth coordination site for the metal ion, both in the solid state and in solution. Regarding the complexes' structures, the pyridine moiety does not significantly affect the flexibility of the macrocyclic shape, as two configurational (cyclam–pyridine)copper complexes (*trans* I and *trans* III) can be synthesised. Finally, the pyridine moiety facilitates the stabilisation of copper(I) complexes and, as a result, helps the mediated electron transfer topological reorganisation of the *trans* III complex into the *trans* I one.

Experimental Section

Syntheses: The metal salts were purchased from Aldrich. All the other reagents were of the highest grade commercially available and used without further purification.

Ligand Synthesis: The ligands $\mathbf{L^1}$ and $\mathbf{L^2}$ were synthesised according to a published procedure.[8]

Preparation of the Copper Complexes

$[Cu\mathbf{L^1}](ClO_4)_2$: Copper perchlorate hexahydrate (130 mg, 0.35 mmol) in methanol (5 mL) was added dropwise to a solution of $\mathbf{L^1}$ (100 mg, 0.32 mmol) in methanol (15 mL). The blue solution was refluxed for 2 h and then concentrated by solvent evaporation. The blue solid complex was precipitated upon addition of diethyl ether, and collected by filtration under vacuum. This solid was further dissolved in acetonitrile and the diffusion of a diethyl ether solution produced blue monocrystals of $[Cu\mathbf{L^1}](ClO_4)_2$, suitable for X-ray analysis. $C_{14}H_{25}Cl_2CuN_5O_8{\cdot}H_2O$ (543.84): calcd. C 30.92, H 5.00, N 12.88; found C 31.06, H 4.72, N 12.70. ESI-MS; *m/z* (%): calcd. for $[Cu\mathbf{L^1}(ClO_4)]^+$ 425, found 425 (100); calcd. for $[Cu\mathbf{L^1}H_{-1}]^+$ 325, found 325 (75).

$[Cu\mathbf{L^2}](ClO_4)_2$ *trans* I: A similar procedure to that described for $[Cu\mathbf{L^1}](ClO_4)_2$ was used. Blue single crystals suitable for X-ray diffraction analysis were obtained by diffusion of diethyl ether in the acetonitrile solution of $[Cu\mathbf{L^2}](ClO_4)_2$. $C_{16}H_{29}Cl_2CuN_5O_8$ (553.88): calcd. C 34.70, H 5.28, N 12.64; found C 34.65, H 5.01, N 12.48. ESI-MS; *m/z* (%): calcd. for $[Cu\mathbf{L^2}(ClO_4)]^+$ 453, found 453 (100); calcd. for $[Cu\mathbf{L^2}H_{-1}]^+$ 353, found 353 (60).

CAUTION: Perchlorate-containing complexes are potentially explosive and appropriate precautions should be in place for their preparation, handling and storage.

$[Cu\mathbf{L^2}](PF_6)_2$ *trans* III: $Cu(CH_3CN)_4PF_6$ (62 mg, 0.17 mmol, white powder) in methanol (5 mL) was added dropwise to $\mathbf{L^2}$ (50 mg, 0.17 mmol) in methanol (10 mL). The solution, which immediately turned blue, was stirred at room temperature in aerobic conditions for 1 d and then concentrated by solvent evaporation. The violet solid complex was precipitated upon addition of diethyl ether, and

collected by filtration. This solid was further dissolved in methanol and the diffusion of a diethyl ether solution produced violet single crystals of $[Cu\mathbf{L^2}](PF_6)_2$, suitable for an X-ray analysis. $C_{16}H_{29}CuF_{12}N_5P_2{\cdot}CH_3OH$ (676.95): calcd. C 30.16, H 4.91, N 10.35; found C 30.29, H 4.73, N 10.45. ESI-MS; *m*/*z* (%): calcd. for $[Cu\mathbf{L^2}(PF_6)]^+$ 499, found 499 (70); calcd. for $[Cu\mathbf{L^2}H_{-1}]^+$ 353, found 353 (100).

Potentiometric Measurements: Potentiometric titrations were carried out with an automatic titrator composed of a microprocessor burette Metrohm Dosimat 665 and a Metrohm pH-Meter 713 connected to a computer. The titration procedure was fully automated.[25] All measurements were performed within a thermoregulated cell at 20.0 ± 0.1 °C under an argon stream to avoid the dissolution of carbon dioxide. The ionic strength was adjusted to 1 with potassium nitrate. The combined "U"-type Metrohm glass electrode used had a very low alkaline error. Solutions of ligand (1×10^{-3} to 2×10^{-3} mol·L^{-1}) and ligand/copper nitrate mixture (ligand/metal ratio in the range 1.2–2) were titrated with a 0.1 mol·L^{-1} KOH solution. For the complex titrations, an equilibration period of 1 month at 40 °C at acidic pH was observed until pH stabilisation. The potentiometric data were processed by using the PROTAF program[9] to obtain the best-fit chemical model and refined overall constants β_{mlh}.

$$m\,M + l\,L + h\,H^+ \rightleftharpoons M_mL_lH_h \qquad \beta_{mlh} = \frac{[M_mL_lH_h]}{[M]^m[L]^l[H^+]^h}$$

The stepwise protonation constants (K_{0lh}) related to the equilibrium of Equation (1) are defined by Equation (2) and were deduced from the refined (β_{0lh}) values by Equation (3).

$$LH_{h-1}^{(h-1)+} + H^+ \overset{K_{0lh}}{\rightleftharpoons} LH_h^{h+} \quad (1)$$

$$K_{0lh} = \frac{[LH_h^{h+}]}{[LH_{h-1}^{(h-1)+}][H^+]} \quad (2)$$

$$\beta_{0lh} = \prod_{i=1}^{h} K_{0li} \quad (3)$$

Spectroscopic Measurements: ^{1}H and ^{13}C NMR spectra were recorded with a Bruker DRX 500 spectrometer. ^{1}H-^{1}H and ^{1}H-^{13}C 2D correlation experiments were performed to assign the signals. In ^{1}H NMR titrations, the pD was adjusted by additions of small amounts of a 4% diluted NaOD solution or a 3.5% diluted DCl solution to D_2O solutions containing ligand $\mathbf{L^1}$ or $\mathbf{L^2}$ (1.5×10^{-3} mol·L^{-1}). The pH was calculated from the measured pD values using Equation (4).[26]

$$pH = pD - 0.40 \quad (4)$$

For both ligands, NMR measurements were performed after an equilibration time of 1 d. Mass spectra in acetonitrile were recorded with a Micromass Q-TOF instrument by electrospray positive ionisation. Electronic spectra in aqueous or acetonitrile solutions were all measured in the 200–900 nm range with a Perkin–Elmer Lambda 6 spectrophotometer. Solid-state spectra were obtained by depositing the complexes on a "Schleicher and Schüll" paper. EPR spectra were recorded with a Bruker ESP 300e spectrometer equipped with a Bruker E035M gaussmeter and an HP 5350B microwave frequency counter. Samples were prepared at a concentration of 5 mmol·L^{-1} in DMF frozen solutions (150 K, Bruker ER4111VT variable-temperature unit). The simulation of the high-field EPR spectra was performed using XSophe software version

Table 7. Crystal data and details of the structure determination for $[Cu\mathbf{L^{1,2}}]^{2+}$complexes.

	$[Cu\mathbf{L^1}](ClO_4)_2$, CH_3CN	$[Cu\mathbf{L^2}]$ *trans* I $(ClO_4)_2$	$[Cu\mathbf{L^2}]$ *trans* III $(PF_6)_2$
Empirical formula	$C_{16}H_{28}Cl_2CuN_6O_8$	$C_{16}H_{29}Cl_2CuN_5O_8$	$C_{16}H_{29}CuF_{12}N_5P_2$
Formula mass	566.88	553.88	644.92
Temperature [K]	120	120	120
Crystal system	monoclinic	monoclinic	monoclinic
Space group	*P*21/*n*	*P*21/*c*	*P*21/*n*
Colour	blue	blue	violet
a [Å]	11.911(5)	9.978(5)	9.2090(2)
b [Å]	13.695(5)	14.867(5)	17.0482(3)
c [Å]	14.837(5)	15.254(5)	15.5835(3)
α [°]	90	90	90
β [°]	98.444	97.635(5)	100.95(10)
γ [°]	90	90	90
Volume [Å^3]	2394(16)	2242(15)	2402.01(8)
Z	4	4	4
$D_{calcd.}$ [g·cm^{-3}]	1.573	1.640	1.783
Absorption coefficient [mm^{-1}]	1.189	1.266	1.152
F(000)	1172	1148	1308
λ(Mo-K_α) [Å]	0.71069	0.71069	0.71073
Largest diff. peak/hole [e·Å^{-3}]	1.719/–1.065	0.566/–0.544	0.952/–0.705
No. independent reflections	5427	7794	5490
No. reflections [$I > 2.0\sigma(I)$]	3924	6564	4527
R_1	0.0641	0.0338	0.0424
wR_2	0.1719	0.0822	0.1078
Goodness-of-fit on F^2	1.006	1.053	1.043

1.1.4 for Mandriva 2006 x86-64 developed by the centre for Magnetic Resonance and the Department of Mathematics of the University of Queensland, Brisbane, Australia, for Bruker Biospin GmbH.[27] The software uses an angular dependence of *g* linewidth model and a Hooke and Jeeves optimisation method with the copper element in a natural abundance (for $[Cu\mathbf{L^1}]^{2+}$: linewidth in the parallel region 23.7×10^{-4} cm^{-1}, in the perpendicular region 19.8×10^{-4} cm^{-1}; for $[Cu\mathbf{L^2}]^{2+}$ *trans* I: linewidth in the parallel region 35.0×10^{-4} cm^{-1}, in the perpendicular region 27.0×10^{-4} cm^{-1}; for $[Cu\mathbf{L^2}]^{2+}$ *trans* III: linewidth in the parallel region 32.5×10^{-4} cm^{-1}, in the perpendicular region 17.5×10^{-4} cm^{-1}).

Electrochemical Measurements: Voltammetric data were recorded with an "Autolab with PGSTAT12" potentiostat (ECO Chemie) associated to a conventional three-electrode electrochemical cell, the working electrode being a glassy carbon disk. A platinum plate was used as a counter electrode and a silver electrode separated from the complex solution was used as a pseudoreference. In acetonitrile, the potential of the pseudoreference was measured versus the ferricinium/ferrocene couple. Complex concentrations were always close to 10^{-3} mol·L^{-1} and tetrabutylammonium hexafluorophosphate 10^{-1} mol·L^{-1} was used as the supporting electrolyte.

Computational Details: The input geometries were obtained by a conformational search performed on each structure, $\mathbf{L^1}$, $[\mathbf{L^1}H^+]$, $[\mathbf{L^1}H^{2+}]$, $[\mathbf{L^1}H^{3+}]$, at the semiempirical level (AM1 calculations, Spartan software[17b]) to determine the lowest conformer for each. The low-energy conformers generated were then minimised using the Gaussian 98 program package.[17a] Both geometry and energy calculations were performed at the DFT/B3LYP/6-31G* level. Each molecular structure was fully optimised and characterised as a minimum by frequency calculations.

Crystal Structure Determination: The crystal diffraction data were collected with a Kappa CCD diffractometer (Centre de Diffractométrie X, Univ. Rennes, France) using monochromated Mo-K_α radiation (λ = 0.71073 Å) at 120 K. Data collection was performed with the COLLECT program.[28] Frames integration and data reduction procedures were realised using the DENZO and SCALEPACK program of the KappaCCD software package, respectively,[29] for the $Cu\mathbf{L^1}$ and $Cu\mathbf{L^2}$ *trans* I/III compounds and with EVAL[30] and SADABS[31] programs. The structures were solved using the direct-methods program SIR97,[32] which revealed all non-hydrogen atoms. SHELXL97[33] was used to refine the structure. Finally, hydrogen atoms were placed geometrically and held in riding mode in the least-squares refinement procedure. Final difference maps revealed no significant maxima. Further details are given in Table 7. CCDC-602318 ($[Cu\mathbf{L^1}]^{2+}$), -602319 ($[Cu\mathbf{L^2}]^{2+}$ *trans* I) and -602320 ($[Cu\mathbf{L^2}]^{2+}$ *trans* III) contain the supplementary crystallographic data for this paper. These data can be obtained free of charge from The Cambridge Crystallographic Data Centre via www.ccdc.cam.ac.uk/data_request/cif.

Supporting Information (see footnote on the first page of this article): Stack plots of ^{1}H NMR spectra (aromatic region), EPR spectra, and Z-matrix of DFT-minimised (B3LYP/6-31G*) lowest-energy conformers.

Acknowledgments

We thank Dr. J. M. Nuzillard and H. Ballia (Université de Reims Champagne Ardenne, France) for their help in the 2D NMR measurements. D. Harakat is thanked for ESI-MS measurements. Prof. G. R. Hanson (University of Queensland, Australia) is gratefully acknowledged for his valuable assistance during the implementation of XSophe.

[1] P. Caravan, J. J. Ellison, T. J. McMurry, R. B. Lauffer, *Chem. Rev.* **1999**, *99*, 2293–2352.
[2] S. Liu, D. S. Edwards, *Bioconjugate Chem.* **2001**, *12*, 7–34.
[3] C. J. Anderson, M. J. Welch, *Chem. Rev.* **1999**, *99*, 2219–2234.
[4] S. J. Paisey, P. J. Sadler, *Chem. Commun.* **2004**, 306–307.
[5] L. Siegfried, T. A. Kaden, *Dalton Trans.* **2005**, 3079–3082.
[6] C. Bucher, J. C. Moutet, J. Pécaut, G. Royal, E. Saint-Aman, F. Thomas, S. Torelli, M. Ungureanu, *Inorg. Chem.* **2003**, *42*, 2242–2252.
[7] C. Amatore, J. M. Barbe, C. Bucher, E. Duval, R. Guilard, J. N. Verpeaux, *Inorg. Chim. Acta* **2003**, *356*, 267–278.
[8] M. Le Baccon, F. Chuburu, L. Toupet, H. Handel, M. Soibinet, I. Déchamps-Olivier, J. P. Barbier, M. Aplincourt, *New J. Chem.* **2001**, *25*, 1168–1174.
[9] a) R. Fournaise, C. Petitfaux, *Talanta* **1987**, *34*, 385–395; b) R. Fournaise, C. Petitfaux, *Analusis* **1990**, *18*, 242–249.
[10] A. Bianchi, M. Micheloni, P. Paoletti, *Coord. Chem. Rev.* **1991**, *110*, 17–113.
[11] R. D. Hancock, R. J. Motekaitis, J. Mashishi, I. Cukrowski, J. H. Reibenspies, A. E. Martell, *J. Chem. Soc., Perkin Trans. 2* **1996**, 1925–1929.
[12] a) Y. Couturier, C. Petitfaux, *Bull. Soc. Chim. Fr.* **1974**, 855–862; b) S. Aoki, D. Kagata, M. Shiro, K. Takeda, E. Kimura, *J. Am. Chem. Soc.* **2004**, *126*, 13377–13390.
[13] G. J. Bridger, R. T. Skerlj, S. Padmanabhan, S. A. Martellucci, G. W. Henson, M. J. Abramo, H. C. Joao, M. Witvrouw, K. De Vreese, R. Pauwells, E. De Clercq, *J. Med. Chem.* **1996**, *39*, 109–119.
[14] C. Bazzicalupi, A. Bencini, E. Berni, A. Bianchi, L. Borsari, C. Giorgi, B. Valtancoli, C. Lodeiro, J. C. Lima, A. J. Parola, F. Pina, *Dalton Trans.* **2004**, 591–597.
[15] K. J. Powell, Academic software Mini SCDatabase, version 5.3, **1999**.
[16] a) L. Frémond, E. Espinosa, M. Meyer, F. Denat, R. Guilard, V. Huch, M. Veith, *New J. Chem.* **2000**, *24*, 959–966; b) M. Meyer, L. Frémond, A. Tabard, E. Espinosa, G. Y. Vollmer, R. Guilard, Y. Dory, *New J. Chem.* **2005**, *29*, 99–108.
[17] a) M. J. Frisch, G. W. Trucks, H. B. Schlegel, G. E. Scuseria, M. A. Robb, J. R. Cheesemen, V. G. Zakrzewski, J. A. Montgomery, R. E. Stratmann, J. C. Burant, S. Dapprich, J. M. Millam, A. D. Daniels, K. N. Kudin, M. C. Strain, O. Farkas, J. Tomasi, V. Barone, M. Cossi, R. Cammi, M. Mennucci, C. Pomelli, C. Adamo, S. Clifford, J. Ochterski, G. A. Petersson, P. Y. Ayala, Q. Cui, K. Morokuma, D. K. Malik, A. D. Rabuk, K. Raghavachari, J. B. Foresman, J. Cioslowski, J. V. Ortiz, B. B. Stefanov, G. Liu, A. Liashenko, P. Piskorz, I. Komaromi, R. Gomperts, R. L. Martin, D. J. Fox, T. Keith, M. A. Al-Laham, C. Y. Peng, A. Nanayakkara, G. Gonzalez, M. Challacombe, P. M. W. Gill, B. G. Johnson, W. Chen, M. W. Wong, J. L. Andres, M. Head-Gordon, E. S. Replogle, J. A. Pople, *Gaussian 98* (Revision A.1), Gaussian Inc., Pittsburgh, PA, **1998**; b) *Spartan04*, Wavefunction, Inc., Irvine, CA.
[18] S. El Ghachtouli, C. Cadiou, I. Déchamps-Olivier, F. Chuburu, M. Aplincourt, V. Turcry, M. Le Baccon, H. Handel, *Eur. J. Inorg. Chem.* **2005**, 2658–2668.
[19] a) A. E. Goeta, J. A. K. Howard, D. Maffeo, H. Puschmann, J. A. Gareth Williams, D. S. Yufit, *J. Chem. Soc., Dalton Trans.* **2000**, 1873–1880; b) V. J. Thorn, C. C. Fox, J. C. A. Boeynes, R. D. Hancock, *J. Am. Chem. Soc.* **1984**, *106*, 3198–3207.
[20] B. Bonisch, C. K. Poon, M. L. Tobe, *Inorg. Chem.* **1965**, *4*, 1102–1108.
[21] B. J. Hathaway, A. A. G. Tomlinson, *Coord. Chem. Rev.* **1970**, *5*, 1–43.
[22] Y. Dong, G. A. Lawrence, L. F. Lindoy, P. Turner, *Dalton Trans.* **2003**, 1567–1576.
[23] K. Miyoshi, H. Tanaka, E. Kimura, S. Tsuboyama, S. Murata, H. Shimizu, K. Ishizu, *Inorg. Chim. Acta* **1983**, *78*, 23–30.
[24] a) C. Bisi Castellani, M. Licchelli, A. Perotti, A. Poggi, *J. Chem. Soc., Chem. Commun.* **1984**, 806–808.

[25] M. Soibinet, I. Déchamps-Olivier, E. Guillon, J. P. Barbier, M. Aplincourt, F. Chuburu, M. Le Baccon, H. Handel, *Eur. J. Inorg. Chem.* **2003**, 1984–1994.
[26] A. K. Covington, M. Paabo, R. A. Robinson, R. G. Bates, *Anal. Chem.* **1968**, *40*, 700–706.
[27] M. Griffin, A. Muys, C. Noble, D. Wang, C. Eldershaw, K. E. Gates, K. Burrage, G. R. Hanson, *Mol. Phys. Rep.* **1999**, *26*, 60–84.
[28] *COLLECT*, KappaCCD software, Nonius BV, Delft, The Netherlands.
[29] Z. Otwinowski, W. Minor in *Methods in Enzymology* (Ed.: C. W. Carter Jr, R. M. Sweet), Academic Press, New York, **1997**, vol. 276, p. 307.
[30] A. Altomare, M. C. Burla, M. Camalli, G. Cascarano, C. Giacovazzo, A. Guagliardi, A. G. G. Moliterni, G. Polidori, R. Spagna, *J. Appl. Crystallogr.* **1999**, *32*, 115–119.
[31] G. M. Sheldrick, *SHELX97*, Program for the Refinement of Crystal Structures, University of Göttingen, Germany, **1997**.
[32] A. J. M. Duisenberg, *Reflections on Area detectors*, Thesis, Utrecht, **1998**.
[33] G. M. Sheldrick, *SADABS*, version 2.03, Bruker AXS Inc., Madison, WI, USA, **2002**.

Received: April 4, 2006
Published Online: July 21, 2006

